REPORT DOCUMENTATION PAGE

Form Approved OMB NO. 0704-0188

1. REPORT DATE (DD-MM-YYYY)	2. REPORT TYPE	3. DATES COVERED (From - To)
02-02-2015	Final Report	1-Jul-2010 - 31-Jul-2014

4. TITLE AND SUBTITLE
Slow light semiconductor laser: Final report

5a. CONTRACT NUMBER
W911NF-10-1-0103

5b. GRANT NUMBER

5c. PROGRAM ELEMENT NUMBER
611102

6. AUTHORS
Amnon Yariv

5d. PROJECT NUMBER

5e. TASK NUMBER

5f. WORK UNIT NUMBER

7. PERFORMING ORGANIZATION NAMES AND ADDRESSES
California Institute of Technology
1200 E. California Blvd.

Pasadena, CA 91125 -0001

8. PERFORMING ORGANIZATION REPORT NUMBER

9. SPONSORING/MONITORING AGENCY NAME(S) AND ADDRESS (ES)
U.S. Army Research Office
P.O. Box 12211
Research Triangle Park, NC 27709-2211

10. SPONSOR/MONITOR'S ACRONYM(S)
ARO

11. SPONSOR/MONITOR'S REPORT NUMBER(S)
57353-EL.9

12. DISTRIBUTION AVAILIBILITY STATEMENT
Approved for Public Release; Distribution Unlimited

13. SUPPLEMENTARY NOTES
The views, opinions and/or findings contained in this report are those of the author(s) and should not contrued as an official Department of the Army position, policy or decision, unless so designated by other documentation.

14. ABSTRACT
A canonical semiconductor laser has photons both generated and stored in the same, optically lossy, III-V material. This leads to an excessive and large amount of noisy spontaneous emission commingling with the laser mode, thereby degrading its coherence. Here, we propose a new design paradigm for the semiconductor laser, where by the incorporation of a very high Q resonator as an integral part of the laser cavity, we demonstrate a semiconductor laser with a spectral linewidth of 18 kHz in the telecom band around 1:55um.

15. SUBJECT TERMS
Semiconductor laser, resonator, Quality factor, Coherence, Narrow linewidth

16. SECURITY CLASSIFICATION OF:			17. LIMITATION OF ABSTRACT	15. NUMBER OF PAGES	19a. NAME OF RESPONSIBLE PERSON
a. REPORT	b. ABSTRACT	c. THIS PAGE			Amnon Yariv
UU	UU	UU	UU		19b. TELEPHONE NUMBER 626-395-4821

Report Title

Slow light semiconductor laser: Final report

ABSTRACT

A canonical semiconductor laser has photons both generated and stored in the same, optically lossy, III-V material. This leads to an excessive and large amount of noisy spontaneous emission commingling with the laser mode, thereby degrading its coherence. Here, we propose a new design paradigm for the semiconductor laser, where by the incorporation of a very high Q resonator as an integral part of the laser cavity, we demonstrate a semiconductor laser with a spectral linewidth of 18 kHz in the telecom band around 1:55um.

Further, the large intracavity field intensity resulting from the high-Q operation gives rise to non-linear effects. We develop a theoretical model based on nonlinear rate equations to study the effect of two-photon absorption and induced free-carrier absorption in silicon on the laser's performance, and compare it to experimental results.

Enter List of papers submitted or published that acknowledge ARO support from the start of the project to the date of this printing. List the papers, including journal references, in the following categories:

(a) Papers published in peer-reviewed journals (N/A for none)

Received		Paper
02/02/2015	7.00	C. T. Santis, S. T. Steger, Y. Vilenchik, A. Vasilyev, A. Yariv. High-coherence semiconductor lasers based on integral high-Q resonators in hybrid Si/III-V platforms, Proceedings of the National Academy of Sciences, (02 2014): 2879. doi: 10.1073/pnas.1400184111
TOTAL:	**1**	

Number of Papers published in peer-reviewed journals:

(b) Papers published in non-peer-reviewed journals (N/A for none)

Received		Paper
TOTAL:		

Number of Papers published in non peer-reviewed journals:

(c) Presentations

Number of Presentations: 0.00

Non Peer-Reviewed Conference Proceeding publications (other than abstracts):

Received		Paper
09/06/2012	3.00	Hsi-Chun Liu, Amnon Yariv. Designing Bessel Filters Based on Coupled-Resonator Optical Waveguides for Dispersion-Free Slow Light, CLEO/QELS,Baltimore,USA,May2011. 01-MAY-11, . : ,
09/06/2012	2.00	Hsi-Chun Liu, Christos Santis, Amnon Yariv. Coupled-Resonator Optical Waveguides (CROWs) Based on Grating Resonators with Modulated Bandgap, Slow and Fast Light (SL),Toronto,Canada,June2011. 12-JUN-11, . : ,
09/06/2012	6.00	Hsi-Chun Liu, Christos Santis, Amnon Yariv. Coupled-resonator optical waveguides (CROWs) based on tapered grating-defect resonatorsrs, CLEO May2012. 06-MAY-12, . : ,
TOTAL:	**3**	

Number of Non Peer-Reviewed Conference Proceeding publications (other than abstracts):

Peer-Reviewed Conference Proceeding publications (other than abstracts):

Received		Paper
02/02/2015	8.00	Yaakov Vilenchik, Christos Santis, Scott Steger, Naresh Satyan, Amnon Yariv. Theory and observation on non-linear effects limiting thecoherence properties of high-Q hybrid Si/III-V lasers, SPIE Photonics West 2015. 09-FEB-15, . : ,
TOTAL:	**1**	

Number of Peer-Reviewed Conference Proceeding publications (other than abstracts):

(d) Manuscripts

Received		Paper
09/04/2012	1.00	Hsi-Chun Liu, Amnon Yariv. Synthesis of high-order bandpass filters based on coupled-resonator optical waveguides (CROWs), Optics Express (08 2011)
09/06/2012	5.00	Hsi-Chun Liu, Amnon Yariv. ”Ideal” optical delay lines based on tailored-coupling and reflecting, coupled-resonator optical waveguideses, Optics Letters (11 2011)
09/06/2012	4.00	Hsi-Chun Liu, Amnon Yariv. Designing coupled-resonator optical waveguides based on high-Q tapered grating-defect resonatorsors, Optics Express (02 2012)
TOTAL:	**3**	

Number of Manuscripts:

Books

Received	Book
TOTAL:	

Received	Book Chapter
TOTAL:	

Patents Submitted

Methods and Systems for Delaying Optical Waves
High-Coherence Semiconductor Light Sources

Patents Awarded

Awards

Graduate Students

NAME	PERCENT_SUPPORTED	Discipline
Liu, Hsi-Chun	0.26	
Steger, Scott	0.16	
Vasilyev, Arseny	0.03	
FTE Equivalent:	**0.45**	
Total Number:	**3**	

Names of Post Doctorates

NAME	PERCENT_SUPPORTED
Naresh Satyan	0.10
Christos Santis	0.20
FTE Equivalent:	**0.30**
Total Number:	**2**

Names of Faculty Supported

NAME	PERCENT_SUPPORTED	National Academy Member
Dr. Amnon Yariv	1.00	Yes
FTE Equivalent:	**1.00**	
Total Number:	**1**	

Names of Under Graduate students supported

NAME	PERCENT_SUPPORTED
FTE Equivalent:	
Total Number:	

Student Metrics

This section only applies to graduating undergraduates supported by this agreement in this reporting period

The number of undergraduates funded by this agreement who graduated during this period: 0.00

The number of undergraduates funded by this agreement who graduated during this period with a degree in science, mathematics, engineering, or technology fields:..... 0.00

The number of undergraduates funded by your agreement who graduated during this period and will continue to pursue a graduate or Ph.D. degree in science, mathematics, engineering, or technology fields:..... 0.00

Number of graduating undergraduates who achieved a 3.5 GPA to 4.0 (4.0 max scale):..... 0.00

Number of graduating undergraduates funded by a DoD funded Center of Excellence grant for Education, Research and Engineering:..... 0.00

The number of undergraduates funded by your agreement who graduated during this period and intend to work for the Department of Defense 0.00

The number of undergraduates funded by your agreement who graduated during this period and will receive scholarships or fellowships for further studies in science, mathematics, engineering or technology fields: 0.00

Names of Personnel receiving masters degrees

NAME

Total Number:

Names of personnel receiving PHDs

NAME
Liu, Hsi-Chun
Total Number: **1**

Names of other research staff

NAME PERCENT_SUPPORTED

FTE Equivalent:
Total Number:

Sub Contractors (DD882)

Inventions (DD882)

Scientific Progress

See Attachment

Technology Transfer

Slow light semiconductor laser: Final report

California Institute of Technology, Pasadena, CA

Contents

1 High coherence semiconductor lasers based on integral high-Q resonators in hybrid Si/III-V platforms

Abstract

The semiconductor laser is the principal light source powering the world-wide optical fiber network. Ever-increasing demand for data is causing the network to migrate to phase-coherent modulation formats, which place strict requirements on the temporal coherence of the light source that can no longer be met by present semiconductor lasers. This failure can be traced directly to the canonical laser design in which photons are both generated and stored in the same, optically lossy, III-V material. This leads to an excessive and large amount of noisy spontaneous emission commingling with the laser mode, thereby degrading its coherence. High losses also decrease the amount of stored optical energy in the laser cavity, magnifying the effect of each individual spontaneous emission event on the phase of the laser field. Here, we propose a new design paradigm for the semiconductor laser. Keys to this paradigm are the maximal removal of stored optical energy from the lossy III-V material by concentrating it in a passive, low-loss material and the incorporation of a very high Q resonator as an integral (i.e., not externally coupled) part of the laser cavity. We demonstrate a semiconductor laser with a spectral linewidth of 18 kHz in the telecom band around $1.55\mu m$, achieved using a single-mode silicon resonator with Q of 10^6.

1.1 Significance statement

The data rate of modern optical fiber communication channels is increasingly constrained by the noise inherent to its principal light source – the semiconductor laser (SCL). Here we examine the phase noise of SCLs due to the spontaneous recombination of excited carriers radiating into the lasing mode as mandated by quantum mechanics. By incorporating a very high-Q optical resonator as an integral part of a hybrid Si/III-V laser cavity, we can remove most of the modal energy from the optically lossy III-V active region thereby reducing the spontaneous emission rate while simultaneously increasing the number of phase-stabilizing stored photons. Our fabricated SCLs boast more

than 10× linewidth improvement compared to commercial SCLs with further major coherence increase possible.

1.2 Introduction

Almost from its inception, there ensued a continuous effort to improve the coherence of the semiconductor DFB laser. The methods employed to this end include: long cavities [1], longitudinal mode engineering via multiple phase-shifts [2, 3], optimization of the active medium (e.g. strained QW) [4], and wavelength detuning [5, 6]. Progress has been hindered by the inevitable penalty paid for the coherence-limiting optical absorption, the result of spatially co-localizing both photons and electrons in a highly absorbing active medium.

The finite coherence of laser light is of fundamentally quantum-mechanical origin, the result of spontaneously generated photons entering the lasing mode from the active region of the laser medium. Under the effect of a large number of independent spontaneous emission events, the laser field phasor performs a random walk in the complex plane, which results in a phase excursion given by [7]

$$\left\langle [\Delta\theta(\tau)]^2 \right\rangle = \frac{N_{\mathrm{th}} W_{\mathrm{sp}}}{2\bar{n}} (1+\alpha^2)\tau, \tag{1}$$

where N_{th} is the number of excited carriers at threshold, W_{sp} is the spontaneous emission rate (s^{-1}) into the lasing mode, $\bar{n}$ is the average number of coherent photons in the lasing mode, α is the linewidth enhancement factor due to coupling of amplitude and phase fluctuations, and τ is the symbol duration (s). The numerator and denominator of equation 1 represent conceptually photon generation and photon storage, respectively. Increasing the quality factor, Q, of the laser cavity provides a double benefit to phase noise by reducing the number of excited carriers needed to reach threshold, thus decreasing spontaneous photon generation, while simultaneously increasing photon storage.

The quality factor of conventional III-V semiconductor lasers is limited by free carrier absorption in the heavily doped p- and n-type cladding regions, as well as in the active region, where photons, both spontaneous and induced, are generated. There is an inevitable compromise resulting from carrying out both photon generation and photon storage in the same III-V material. While III-V is needed for gain, its high absorption makes it unsuitable for photon

storage. Heterogeneous Si/III-V integration [8, 9, 10, 11] allows lossy III-V material to be replaced with low-loss silicon without significantly changing the properties of the optical mode. The total Q of a hybrid Si/III-V resonator can then be expressed as

$$\frac{1}{Q} = \frac{\Gamma}{Q_{\text{III-V}}} + \frac{1-\Gamma}{Q_{\text{Si}}}. \tag{2}$$

where Γ is the mode confinement factor in III-V, $Q_{\text{III-V}}^{-1}$ is the absorption-dominated loss in III-V, and Q_{Si}^{-1} is the loaded Q of a passive Si-only resonator (figure 1c). Absorption losses in high resistivity Si are typically three orders of magnitude lower than in III-V, so replacing excess III-V material with silicon creates a large potential improvement to laser coherence. This potential can only be realized by maximizing the total Q of the resonator (i.e. making $Q_{\text{Si}} \gg Q_{\text{III-V}}$). Hybrid Si/III-V thus opens a new regime in which absorption losses are no longer necessarily dominant and other components of loss, previously only relevant in high-Q passive resonator design, must be addressed to maximize the coherence of a semiconductor laser.

Additionally, manipulating the transverse geometry of the hybrid Si/III-V waveguide alters the modal confinement between the lossy III-V and the low-loss silicon [12]. Engineering the waveguide mode to decrease Γ has two effects on laser coherence: (1) the cavity Q increases according to equation 2, thus improving photon storage, $\bar{n}$, and (2) the intensity of the laser mode in the active region decreases, decreasing the spontaneous emission rate into this mode, W_{sp}. Removing light from III-V appears counterintuitive because it reduces the modal gain available to the laser; however, in the limit that the $Q_{\text{III-V}}$ term of equation 2 dominates the total Q, the reduction in modal gain is exactly balanced by a reduction in total modal loss and thus the threshold carrier density remains constant.

It thus emerges that Q_{Si} is the factor limiting how much light can be removed from III-V and is the focus of the work presented here. The design paradigm following from equation 2 shifts the focus of laser design from optimization of the active material to optimization of a high-Q passive resonator, independent of the gain medium used.

1.3 High-Q cavity design

Designing the laser's high-Q integral resonator is constrained by its role of determining the oscillation frequency and the longitudinal mode profile. To

maximize the resonator Q, subject to these constraints, it is instructive to conceptually separate Q_{Si} into its constituent optical loss mechanisms [13]:

$$\frac{1}{Q_{\mathrm{Si}}} = \frac{1}{Q_{\mathrm{rad}}} + \frac{1}{Q_{\mathrm{abs}}} + \frac{1}{Q_{\mathrm{sc}}} + \frac{1}{Q_{\mathrm{e}}}. \tag{3}$$

Losses due to radiation (Q_{rad}^{-1}), absorption (Q_{abs}^{-1}) and scattering (Q_{sc}^{-1}) comprise the intrinsic component of losses in Si. Added to it is the resonator loading, Q_{e}^{-1} (i.e. external coupling), which determines the fraction of stored energy that is tapped as useful output through the laser mirrors. There is inevitably a trade-off in laser design between large stored energies, necessary for narrow linewidths, and useful output.

The high-Q Si resonator is fashioned from a silicon waveguide patterned with a 1D grating (figure 1c). Coupling to radiation modes (Q_{rad}^{-1}) is minimized via a bandgap-modulated defect section in the middle of an otherwise uniform grating [14, 15, 16, 17], as shown in figure 2a. The defect is designed directly in the frequency domain by parabolically modulating the lower frequency band edge of the grating as a function of position along the resonator (figure 2b). This quadratic modulation acts as a potential well, localizing a resonant mode with a Gaussian-like profile in both real and reciprocal space (figures 2d,e), similar to the ground state electron wavefunction in a quantum harmonic oscillator. By appropriately choosing the well depth V, defined as an offset frequency from the uniform grating band edge, and its spatial width L_{d}, the mode can be localized tightly in k-space, thereby greatly reducing coupling to the continuum of radiation modes (figure 2e). To fabricate a device, the frequency band edge profile is translated to a grating structure modulation by varying the transverse width W_{y} of etched holes along the length of the resonator (Fig. 2a).

To minimize scattering loss (Q_{sc}^{-1}) we choose a shallow rib geometry for the waveguide, to "bury" the mode in the Si slab and thus isolate it from the roughness of the etched sidewalls (figure 1). Absorption losses in Si are small compared to the other sources of loss in silicon and therefore can be neglected.

Uniform grating reflectors of length L_{m} on either side of the defect determine the fraction of the total power generated in the active region that is coupled as useful output, and therefore the external loading of the resonator (Q_{e}). Since we seek to maximize the total loaded Q to reduce phase noise, high-Q hybrid resonators are designed to be significantly undercoupled (i.e., in the limit of high Q_{e}). Conventional DFB lasers in this loading

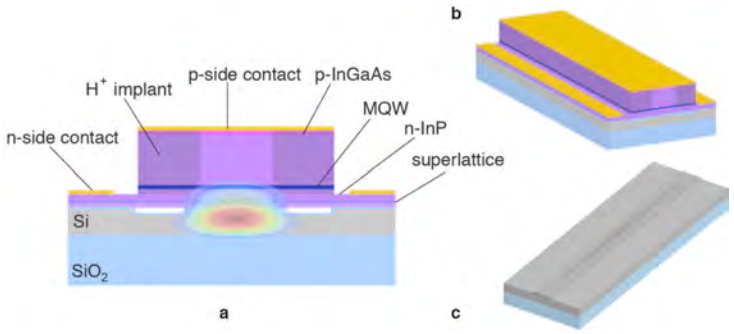

Figure 1: **High-Q hybrid laser device schematics (not to scale). a,** Two-dimensional cross section of the hybrid platform, with superimposed optical transverse mode profile. **b,** Perspective view of a high-Q hybrid laser. **c,** Perspective view of the high-Q Si resonator.

regime become susceptible to spatial hole burning-induced mode instability and linewidth rebroadening due to their sharply-peaked spatial mode profile [18, 19]. In the high-Q hybrid laser, spatial hole burning is mitigated by the broad Gaussian longitudinal mode profile, thus allowing considerable undercoupling and, therefore, large stored energies in the cavity.

1.4 Results

To determine the Q_{Si} metric for the resonators utilized in this work, we fabricated and tested passive Si resonators of the same type and scale as the hybrid, only without the III-V attached. We measured loaded quality factors for these resonators exceeding 10^6 (figure 2g), which represent record high Q for 1D photonic crystal waveguide resonators on Si-on-insulator (SOI). In the hybrid lasers, the confinement factor in III-V is fixed at $\Gamma = 15\%$ and realized with a silicon device layer 500 nm thick.

We fabricated high-Q hybrid lasers using standard e-beam lithography and plasma etching to create low-loss gratings on Si, followed by die-scale direct bonding to the III-V material. Details of the fabrication process can be found in the Methods section. The hybrid Si/III-V resonators are based on photonic wells with design parameter set of ($V = 100\,\mathrm{GHz}$, $L_{\mathrm{d}} = 200\,\mu\mathrm{m}$), which results in a single localized defect mode. Fourier analysis for the selected design parameter set yields an estimate of $Q_{\mathrm{rad}} \sim 10^7$. The length of the distributed Bragg reflectors on either side of the defect is set to significantly undercouple the resonator, with calculated $Q_{\mathrm{e}} \approx 5 \times 10^6$, based on the

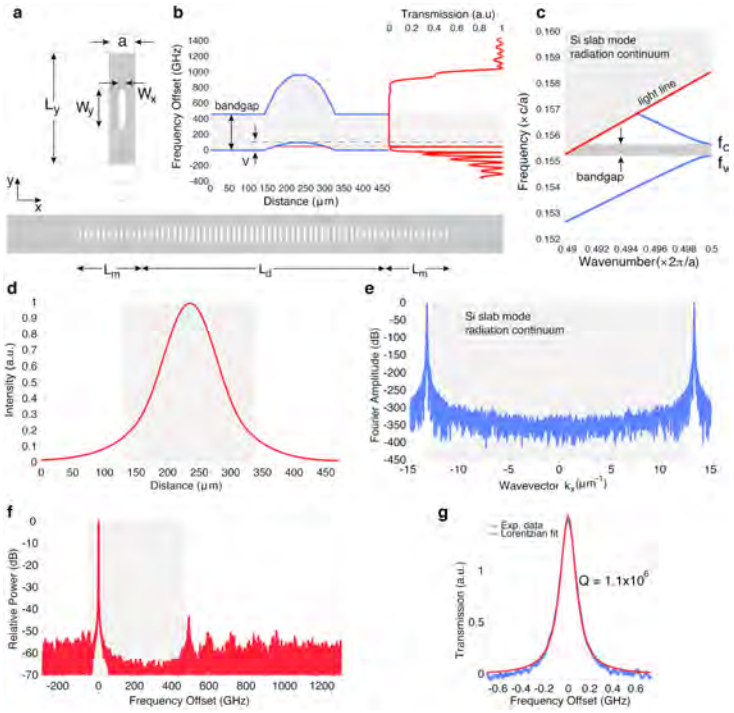

Figure 2: **Design features of the high-Q hybrid resonator. a,** Top view of the geometry of the grating in Si. **b,** Spatial band structure of a high-Q hybrid resonator plotted against the simulated transmission spectrum. Example shown for design parameters $V = 100\,\mathrm{GHz}$, $L_\mathrm{d} = 200\,\mu\mathrm{m}$, W_y from 200 nm to 600 nm. **c,** Dispersion diagram of a local unit cell. Eigenfrequencies f_v, f_c correspond to modulated frequency distribution $f_\mathrm{v}(x)$, $f_\mathrm{c}(x)$ of the resonator spatial band structure. **d,** Simulated profile of the longitudinal field intensity of a high-Q hybrid resonator. The grey-shaded area denotes the defect section of the resonator. **e,** Fourier component amplitude distribution of the longitudinal field of a high-Q hybrid resonator. The grey-shaded area denotes the continuum of radiation modes. **f,** Simulated emission spectrum of a high-Q hybrid laser. The grey-shaded area denotes the resonator bandgap. **g,** Experimental trace and Lorentzian fit of the transmission resonance of a high-Q Si resonator. (Structure design parameters used in all of the above simulations: $L_y = 2.0\,\mu\mathrm{m}$, $W_\mathrm{x} = 90\,\mathrm{nm}$, $a = 235\,\mathrm{nm}$.)

assumption of a predominantly III-V absorption-limited intrinsic Q for the resonator. Typical cavity lengths, including the reflectors, are in the range of 1 mm.

High-Q hybrid lasers are tested unpackaged on a temperature controlled stage. We obtain single-mode, continuous-wave laser operation with threshold currents as low as 30 mA and single-side output powers as high as 9 mW at room temperature (20 °C) (figure 3b). Lasing occurs over temperatures spanning the range of 10 °C to 75 °C (figure 3a). Single-mode oscillation is observed over a wavelength span of 45 nm (1530 nm to 1575 nm), in lasers with different grating periods (a from 230 nm to 240 nm). Figure 3c shows a representative optical spectrum of a high-Q hybrid laser. Side mode suppression ratios better than 50 dB are obtained at each operating wavelength (figure 3d). The experimental optical spectrum agrees with simulated spectra for both the passive (figure 2b) and active (figure 2f) resonators. The lasing mode appears, as predicted from simulation, near the low frequency band edge (offset $\sim$ 60 GHz), while the strongest side mode is just outside the low frequency band edge.

To characterize the temporal coherence of the high-Q hybrid laser, we measure the spectral density of the frequency fluctuations [20] as described in Methods. This avoids the ambiguity of the traditional self-heterodyne measurement method in discriminating between low frequency (e.g. $1/f$) and high frequency noise contributions to the spectral linewidth [21]. By displaying this noise as a function of frequency, we can separate the individual noise mechanisms. We are especially interested in the high frequency components of the noise spectrum, since this portion of the spectrum affects high-data rate optical communications [22].

Figure 4 shows a typical frequency noise spectrum of a high-Q hybrid laser. Two distinct regions in the plot can be discerned. The first, up to approximately 100 kHz, displays a $1/f$-type dependence, while a second segment with a gentler slope extends up to 100 MHz. The trend of Fig. 4 is representative of all the high-Q hybrid lasers tested. The observed frequency noise spectrum is largely dominated by noise of technical origin (e.g. laser driving electronics). Since our data do not display a level white noise floor, we can only place an upper bound on the spontaneous emission-induced phase noise. This upper bound can be expressed in terms of a spectral linewidth (i.e. modified Schawlow-Townes linewidth) by using the value of the spectral density at the high-frequency end and multiplying it by 2π for the two-sided spectra measured in this work [23, 24]. The narrowest linewidth attained is

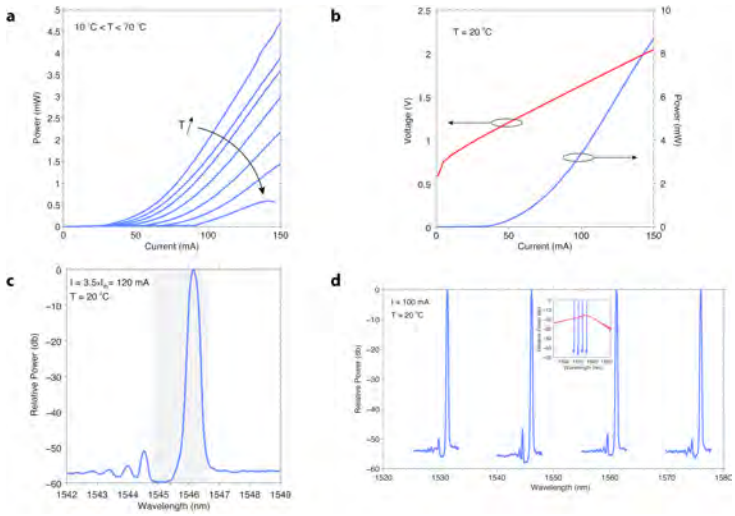

Figure 3: **High-Q hybrid laser characterization results. a,** Light vs. pump current (L-I) curves as a function of the operating temperature, taken from a representative laser. **b,** L-I and current vs. forward voltage (I-V) curves for a high-Q hybrid laser measured at room temperature (20 °C), taken from the laser with the highest one-sided output power. **c,** OSA-limited optical spectrum of a high-Q hybrid laser at a pump current of 120 mA ($3.5 \times I_{\mathrm{th}}$) at 20 °C, demonstrating sidemode suppression of 50 dB. The grey-shaded area denotes the bandgap. **d,** OSA-limited optical spectra of high-Q hybrid lasers of varying grating period taken at 120 mA ($3.5 \times I_{\mathrm{th}}$) and 20 °C, demonstrating continuous-wave, single-mode lasing from 1530 nm to 1575 nm (C-band), with side mode suppression ratios over 50 dB. The inset shows the relative position of the four spectra with respect to the spontaneous emission spectrum below threshold.

18 kHz, measured at a pump current of $4.5 \times I_{\mathrm{th}}$ (160 mA).

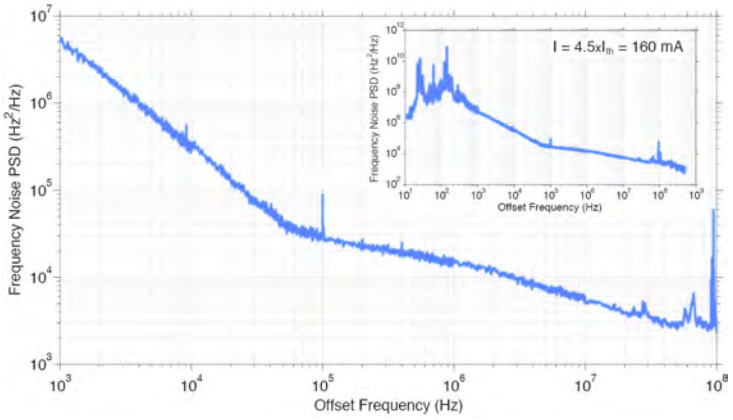

Figure 4: **Frequency noise spectrum of the lowest-noise high-Q hybrid laser**. The measurement is taken at a pump current of 160 mA ($4.5 \times I_{\mathrm{th}}$) at 20 °C. Spikes at 100 kHz and 100 MHz correspond to current source electronic noise and FM radio noise respectively. A spectral linewidth of 18 kHz can be calculated for this laser by multiplying the PSD value near 100 MHz by 2π. The inset includes the full frequency noise spectrum, showing the feedback-suppressed low frequency end of the spectrum as well as the onset of the MZI roll-off (FSR = 847 MHz).

Figure 5a presents the extracted spectral linewidth of a representative high-Q hybrid laser as a function of the normalized pump current offset from threshold. The linewidth decreases with increasing pump current, reflecting the increase in the total number of photons, $\bar{n}$ stored in the laser resonator. Immediately above threshold ($1.1 \times I_{\mathrm{th}}$), the high-$Q$ hybrid laser exhibits sub-MHz scale linewidths. These linewidths near threshold are much narrower than those of comparable narrow-linewidth semiconductor lasers at the same pump power [25] (see also supplementary information), demonstrating that it is the enhanced cavity Q and not strong pumping behind the superior coherence characteristics of the high-Q hybrid lasers. With further increase of the current, the linewidth decreases by more than an order of magnitude. Deviation from the expected linewidth dependence on pump current is observed in the form of a linewidth floor. This deviation is due to increased side mode competition [26] observed in the optical spectra of the lasers and probably caused by spatial hole burning. Narrow-linewidth performance is demonstrated across the entire C-band (figure 5b), obtained from lasers with varying grating period and spanning different chips and laser bars.

The ultimate linewidth of a semiconductor laser made using this paradigm

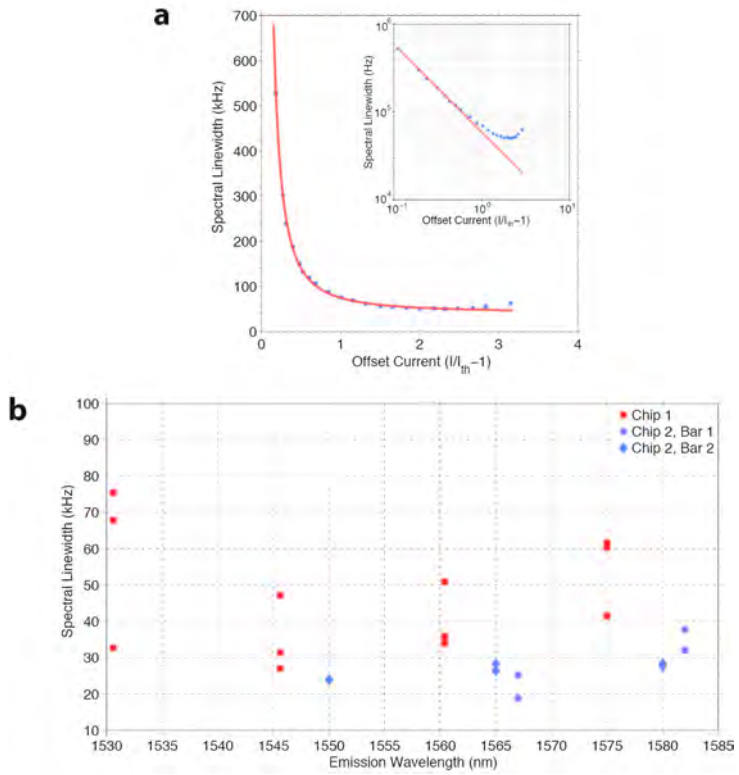

Figure 5: **Linewidth characterization of high-Q hybrid lasers. a,** Spectral linewidth of a single high-Q hybrid laser as a function of the offset pump current from threshold ($I_{\mathrm{th}} = 35\,\mathrm{mA}$) 20 °C, taken from a representative laser. The inset shows the same dependence in log-log scale. **b,** Distribution of the spectral linewidth of high-Q hybrid laser tested spanning 3 laser bars fabricated on 2 separate chips, as a function of their emission wavelength.

is limited by two factors: the state-of-the-art in passive resonators and the fraction of the optical energy stored in III-V. Previously-reported linewidths for hybrid Si/III-V DFB lasers are on the order of a few MHz (3.6 MHz[10]). The high-Q of the lasers reported here enables linewidths approximately 200$\times$ narrower than the those previously reported, though Γ is comparable in both designs. Further linewidth reduction beyond the 18 kHz reported here would be possible if, according to equation 2, the total cavity Q was increased, by increasing Q_{Si} and/or decreasing Γ. With the $Q_{\mathrm{Si}} = 10^6$ achieved in this work, further decreasing Γ would give an additional factor of 10 reduction in linewidth, without affecting threshold.

We have proposed a new paradigm for the design of high-coherence semiconductor lasers, demonstrated here with a spectral linewidth of 18 kHz. Our approach circumvents historical limitations of laser design and it raises the bar on the ultimate coherence of semiconductor lasers. The new figure of merit for coherence introduced in this work is the quality factor of the integral passive resonator, which is subject to the methods and techniques utilized. Yet, the paradigm itself is more generic than the specific tools employed. These merely reflect the present state-of-the-art in technology, and it is entirely likely that as technology, materials, and design methods advance, other methods to design high-Q passive resonators will emerge, to further push the coherence limits.

1.5 Materials

We pattern the passive resonator with e-beam lithography (Vistec EBPG 5000+, Zeon ZEP 520A resist) and transfer the pattern to silicon with a pseudo-Bosch process (Oxford 380). To turn the passive resonator into a high-Q hybrid laser, we smooth the waveguide sidewalls to improve Q_{sc} by growing 15 nm of dry thermal oxide (oxidation times calculated using the Massoud model). We strip the oxide with HF (Transene Buffer HF-Improved), and regrow 20 nm of dry oxide. The silicon chip is prepared for direct wafer bonding through acetone and IPA cleans followed by an organic strip in Nanostrip (Cyantek) for 1 m. An unpatterned III-V chip with an epi-structure given in the Supplementary Information is prepared through acetone and IPA cleans followed by NH_4OH:H_2O 1:15 for 10 m. Both chip surfaces are activated for bonding with 5 "treatments" (5 passes at 25 mm/s) in oxygen plasma at 200 W (Suss NP12). The chips are directly bonded by bringing them into contact and applying light pressure with tweezers. We are

uncertain if bonding is spontaneous or induced by the pressure. The bonded chips are annealed at 150C for 1 h followed by 285C for 5 h. After bonding, the InP handle is removed in HCl:H_2O 1:3. We use ion implantation (H^+, 170 keV, 5e14 cm^{-2}) and an AZ5214E mask to define a current path above the silicon waveguide. We form the p-contact to p^+-InGaAs above the current path by depositing Ti/Pt/Au (20 nm/50 nm/150 nm) and lifting off image-reversed AZ5210 resist. The III-V mesa is created by wet etching down to the n-contact layer (piranha H_2SO_4:H_2O_2:H_2O 1:1:10 7 s, HCl:H_2O 1:2 17 s, piranha 45 s). We form the n-contact to n^+-InP by depositing Ge/Au/Ni/Au (30 nm/50 nm/12 nm/225 nm). The die is thinned to 150 µm and cleaved into bars. Individual bars are annealed at 325 °C for 30 s. We anti-reflection coat the bars on both facets with 250 nm Al_2O_3.

Passive Si resonators are characterized by measuring their frequency response in transmission mode. To speed up data acquisition and improve resolution, necessary to measure narrow resonances, we employ a tunable laser (Santec TSL-510, 1570 nm to 1590 nm), configured as a fast, optoelectronically controlled frequency sweeping source [27] to interrogate the resonators. For calibration of the frequency sweep, part of the laser source is transmitted through a Mach-Zehnder interferometer (MZI), the output of which is used to convert the resonator's temporal response to the frequency domain. Loaded quality factors are calculated by Lorentzian fitting of the transmission resonances.

We measure frequency noise by employing a MZI as a frequency discriminator, with a differential delay shorter than the expected laser coherence time. The corresponding MZI free-spectral range (FSR) is 847 MHz. The interferometer converts laser phase fluctuations to intensity fluctuations when biased at quadrature and measured with a high-speed photodetector, the spectrum of which is obtained on an RF spectrum analyzer. The choice for the interferometer delay is a trade-off between frequency scan range and frequency gain. For this method to yield accurate results, the interferometer must remain at quadrature for the duration of a high-resolution measurement of the frequency spectrum. The hybrid lasers under test, not being packaged, are particularly sensitive to environmental temperature fluctuations, causing the laser center frequency to drift out of quadrature. We lock the interferometer in quadrature with negative electronic feedback to the laser's pump current. The feedback loop bandwidth is kept below 100 Hz, sufficient to suppress low-frequency temperature-induced fluctuations, while leaving the higher-frequency noise spectrum unaffected.

2 Non-linear effects limiting the coherence properties of high-Q hybrid Si/III-V lasers

Hybrid Si/III-V is a promising platform for semiconductor narrow-linewidth lasers, since light can be efficiently stored in low loss silicon and amplified in III-V materials. The introduction of a high-Q cavity in silicon as an integral part of the laser's resonator leads to major reduction of the laser linewidth. However, the large intracavity field intensity resulting from the high-Q operation gives rise to non-linear effects. We present a theoretical model based on non-linear rate equations to study the effect of two-photon absorption and induced free-carrier absorption in silicon on the laser's performance. The predictions from this model are compared to the experimental results obtained from narrow-linewidth lasers fabricated by us. It is shown to have an effect on the linearity of the L-I curve, and to reduce the achievable Schawlow-Townes linewidth.

The conventional semiconductor laser (SCL) design strategy that uses monolitically grown III-V materials for both electron and photon storage is fundamentally inconsistent with high coherence, i.e., narrow-linewidth, operation. Electrical current flows through the same volume which is occupied by the optical mode in order to inject carriers into the the quantum wells (QW). This imposes the use of optically-absorbing doped III-V layers which limit the achievable laser's quality factor (Q). Since the laser linewidth is proportional to Q^2, conventional SCLs are historically limited to sub-MHz linewidth.

Hybrid Si/III-V lasers have been demonstrated by several groups[28, 29, 30, 31]. The main motivation for these devices is the generation of laser light on silicon platforms, close to high-speed silicon-based electronics or other silicon-photonics devices. In our case we use the silicon as part of the resonator and re-design the mode in such a way that the overwhelming majority (>97%) of the optical energy now resides in silicon. This results directly in orders of magnitude improvement in the resonator mode quality factor. It was recently demonstrated that this new design paradigm[31], shown in Fig. 6, is essential to minimizing spontaneous emission into the laser mode thus improving, by orders of magnitude, the coherence of the laser field. The losses in the Si rather than in the III-V now set the limit on coherence. The reduction in modal gain is precisely balanced by the reduction in modal

loss, and laser conditions (gain = loss) are achieved without compromising threshold current.

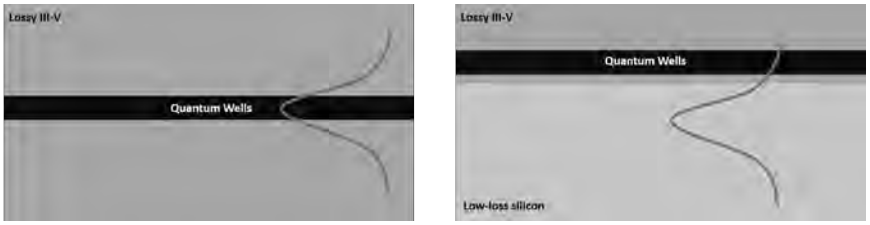

(a) (b)

Figure 6: (a) Conventional SCL design. (b) High Coherence Si/III-V design

Passive micro Si resonators with quality factors close to or bigger than a million were reported in the literature [32, 31] . These integrated Si-based implementations yield small cavity sizes, compared to commercial low-linewidth lasers. The incorporation of such a high-Q Si resonator in the hybrid Si/III-V platform was demonstrated to yield lasers with linewidth as low as 18 KHz [31] . The high intra-cavity field intensities that are a consequence of the high-Q and the small cavity size enhance the probability of non-linear multi-photon processes. Two-photon absorption (TPA) and induced free-carrier absorption (FCA) were shown to alter the propagation of intense pulses[33] , to suppress RIN[34] and to produce all-optical-modulation[35] . In this paper we investigate these non-linear processes in the context of high-Q semiconductor lasers.

Si has a large non-linear $\chi^{(3)}$ coefficient compared to commonly used low-loss materials such as SiO_2 or Si_3N_4. When the field intensity builds up in the presence of gain, non-linear processes, such as TPA and subsequent FCA, add extra loss[36] , that would otherwise be negligible in the low-intensity passive version of the same resonator. In our laser design, in which the high optical energy is stored in a Si micro-resonator, the achievable cavity's quality factor may be limited due to non-linear loss.

We analyze the effect of these non-linear phenomena on the laser performance by including TPA and FCA in a modified version of the rate equations.

In general, the optical mode and electron density profile vary along the resonator's volume. However, in order to numerically investigate non-linear laser-dynamics, it is advantageous to simplify the model. To that end, we neglect all spatial variations and approximate our mode as constant within a rectangular box. The size of the box will be equivalent to the FWHM volume

of the mode, and the amplitude will be taken as the average amplitude within that rectangle.

The Electron density in the QWs will also be taken constant within a box. As shown in Fig. 7, two dimensions (x and z axes) of the electron-occupied volume will correspond to the optical cavity box, since we are only interested in the QW electrons that have significant contribution to the modal gain. The third dimension (y) will represent the thickness of the QW layer since the optical mode is approximately fixed over nm scale (compare to Fig. 6).

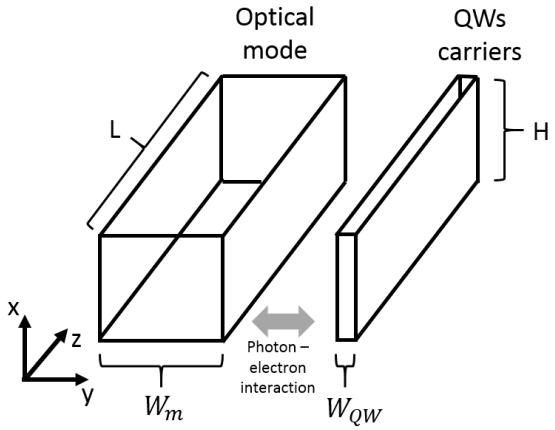

Figure 7: Flat mode approximation for the optical mode and the electron density

The interaction strength between photons and electrons will be calculated using the overlap integral for TE modes[37]:

$$\Gamma_i = \frac{\int_i n_i(\mathbf{r})|E(\mathbf{r})|^2 d^3\mathbf{r}}{n_{eff}\int_{all}|E(\mathbf{r})|^2 d^3\mathbf{r}} \tag{4}$$

Where n_{eff} is the mode's effective index, and the index i represents the desired region (QW in this case). The rate of generation (absorption) of the total number of photons N_p in the box will be calculated using the material gain (loss) G_m, which depends on the QW electron density n_e:

$$\frac{dN_p}{dt} = \Gamma_{QW} G_m(n_e) N_p \tag{5}$$

Optical Kerr effect in Silicon is responsible for intensity-dependant changes of the refractive index. TPA is manifested as the imaginary part of the index

of refraction, and is non-zero whenever the photon's energy is larger than half the band-gap of silicon, as in the case of telecom wavelengths. TPA can be quantified using the coefficient β_T , which relates the change of the imaginary part of the refractive index Δn_i to the field's intensity I using[38]:

$$\Delta n_i = \frac{c}{2\omega}\beta_T I \tag{6}$$

Where c is the velocity of light, and ω is the angular optical frequency. The coefficient β_T is wavelength-dependent, and its value at $1.55\mu m$ has been measured by several authors[39, 40, 41] .

Optical loss induced by two-photon absorption can be described by a non-linear rate equation term for the average photon density n_p:

$$\frac{dn_p}{dt} = -\beta_T h\nu v_g^2 M_{TPA}\Gamma_{Si}^2 n_p^2 \tag{7}$$

Where $h\nu$ is the photon energy, v_g the group velocity and Γ_{Si} is the confinement factor in Si, defined as in eq. 4 with layer i being the Si layer. The factor M_{TPA} captures the difficulty of describing non-linearities using a flat average-intensity model: Since TPA is proportional to the local density *squared*, it is much stronger at the mode's local peak than at its average over the modes volume V_p. M_{TPA} is defined to ascertain the flat-mode-approximation will not yield gross under-estimation of TPA processes:

$$M_{TPA} = V_p \frac{\int_{Si} |E(\mathbf{r})|^4 d^3\mathbf{r}}{\left(\int_{Si} |E(\mathbf{r})|^2 d^3\mathbf{r}\right)^2} \tag{8}$$

For each TPA absorption event in Si, an electron-hole pair is generated. Long carrier recombination life time of conduction-band electrons in intrinsic silicon allows these carriers to accumulate and interact with the electromagnetic field. This interaction induces both extra loss through plasma effect FCA and refractive index changes. The strength of these effects can be well modeled using the Drude model[42] where the loss coefficient per unit distance α_{FCA} and refractive index change n_{FCA} can be directly related to the electron and hole concentrations n_{Si} and p_{Si} respectively. For intrinsic silicon we can use the parameter[38] σ_a to relate loss rate to electron concentration:

$$\alpha_{FCA} = \sigma_a n_{Si} \tag{9}$$

The changes in refractive index due to free carriers in Si, at $\lambda = 1550$nm, can be described using[38]:

$$n_{FCA} = -8.8 \cdot 10^{-22} n_{Si} - 8.5 \cdot 10^{-18} p_{Si}^{0.8} \tag{10}$$

To estimate the number of free electrons in the steady state operation of the laser we need to solve the diffusion-recombination-generation equation for our specific waveguide geometry. As the bulk recombination time of Si is in the order of a few μsec , the lifetime will be dominated by surface and interface recombination. For a typical laser bar of length and width of a few millimeters, we can neglect surface recombination from distant facets and edges of the bar. The dominant source of electron annihilation would be surface recombination along the interface of the Si slab, which is of sub-micrometers thickness. Therefore we can approximate the 3-dimensional structure using a two dimensional equation[43]:

$$\frac{dn_{Si}}{dt} = \frac{\beta_T h\nu v_g^2}{2} n_p^2 - \frac{n_{Si}}{\tau_b} + D_a \frac{d^2 n_{Si}}{dx^2} - 2\frac{S}{H} n_{Si} \tag{11}$$

Where τ_b is the bulk recombination lifetime in Si, D_a is the ambipolar diffusion coefficient, S is the surface recombination velocity and H is the Si slab thickness. Once we have numerically solved this equation for given photon density profile we can define an effective lifetime for carriers in Si for the given optical mode:

$$\tau_{eff} = \frac{2}{\beta_T h\nu v_g^2 n_p^2} \frac{\int n_{Si}(x) n_p(x) dx}{\int n_p(x) dx} \tag{12}$$

The parameter τ_{eff} describes the average time in which generated electrons interact with the optical mode before they recombine at the surface, the bulk or diffuse away from the mode's area. For micro scale structures the exact value of this parameter is usually dominated by the quality and size of surfaces and interfaces in Si. Typical values in the literature are around $\tau_{eff} = 1$ns[43]. However, since high-Q resonators require high quality interfaces and etched surfaces we expect the effective lifetime to be higher than the normally encountered values.

The SCL rate equation can now be modified to take into account TPA and FCA. Since TPA is a non-linear process that scales with the intensity of the light in the cavity, rather then the total photon energy, it is natural

to express the rate equations in terms of the electron and photon densities. In the total numbers description the stimulated emission process conserves electrons/photons, i.e., radiative recombination of one QW electron generates exactly one photon, and vice versa. Referring to Fig. 7, the rate of the total electron and photon number can be converted to densities by dividing by the volume of the QW and optical cavity respectively. It is useful to define a geometrical confinement factor:

$$\Gamma_{geom} = \frac{W_{QW}}{Wm} \tag{13}$$

The low losses due to the high-Q resonator enables the laser to operate close to transparency. This allows us to write the material gain using the approximate linear expression:

$$G_m = 2v_g G_m^{'}(n_e - n_{tr}) \tag{14}$$

without losing much accuracy. $G_m^{'}$ is the material differential gain and n_{tr} is the transparency carrier density. The optical energy loss rate α in the cavity is expressed using the loaded quality factor Q:

$$\alpha = \frac{2\pi\nu}{Q} \tag{15}$$

The reduced QW confinement factor Γ_{QW} , which is a characteristic of our high-Q platform, minimizes spontaneous emission rate into the mode. The rate can be expressed as:

$$R_{sp} = \frac{\Gamma_{QW} G_m(n_e) n_{sp}}{V_p} \tag{16}$$

Where V_p is the effective mode volume and n_{sp} is the population inversion factor. Eq. 16 is a consequence of a fundamental relationship between stimulated and spontaneous emission[44] .

We can now express the systems of rate equations as:

$$\frac{dn_e}{dt} = -\frac{n_e}{\tau_r} - \frac{\Gamma_{QW}}{\Gamma_{Geom}} G_m(n_e) n_p + \frac{\eta I}{qV_{QW}} \tag{17}$$

$$\frac{dn_p}{dt} = \left(\Gamma_{QW} G_m(n_e) - \alpha\right) n_p - \beta_T h\nu v_g^2 M_{TPA} \Gamma_{Si}^2 n_p^2 - v_g \sigma_a n_{Si} \Gamma_{Si} n_p + R_{sp} \tag{18}$$

$$\frac{dn_{Si}}{dt} = \frac{1}{2}\beta_T h\nu v_g^2 M_{TPA} \Gamma_{Si} n_p^2 - \frac{n_{Si}}{\tau_{eff}} \tag{19}$$

Symbol	Description	Value	Units
τ_r	Recombination life time	$50 \cdot 10^{-9}$	sec
G_m	Material gain	eq. 14	sec^{-1}
$G_m^{'}$	Differential material gain	$1 \cdot 10^{-19}$	m^2
n_{tr}	QWs transparency density	$2 \cdot 10^{24}$	m^{-3}
η	Quantum efficiency	0.3	-
I	Pump current	(sweep)	Amper
q	Electron charge	$1.6 \cdot 10^{-19}$	Coul.
V_{QW}	Quantum well effective volume	$4.2 \cdot 10^{-17}$	m^3
V_p	Effective mode volume	$6 \cdot 10^{-16}$	m^3
α	Linear loss rate in the cavity	eq. 15	sec^{-1}
Γ_{QW}	QW confinenmt factor	eq. 4	-
Γ_{geom}	Geometrical confinement factor	0.07	-
v_g	Mode's group velocity	$c/3.53$	$\frac{\text{m}}{\text{s}}$
β_T	TPA coefficient	$5 \cdot 10^{-12}$[39, 40, 41]	$\frac{\text{m}}{\text{W}}$
M_{TPA}	TPA magnification factor	eq. 8	-
σ_a	FCA cross section	$1.45 \cdot 10^{-21}$[38]	m^2
Γ_{Si}	Si confinement factor	eq. 4	-
R_{sp}	Spontaneous modal emission rate	eq. 16	sec^{-1}
τ_{eff}	Si carriers effective lifetime	$30ns^1$	sec

Table 1: Parameters used for rate equations

The parameters used for the rate equations analysis are summarized in table 1.

The non-linear rate equations 17, 18 and 19 can be solved in the steady state by setting all $\frac{d}{dt} = 0$. The numerical solution of the system of equations can provide insights on the effect of TPA and FCA on laser performance.

Output coupling of lasers with different resonators' quality-factors can in general vary. Even in lasers with the same intrinsic Q, the mirror grating can be adjusted to change the total Q, and the output coupling. In order to compare different laser designs, we will assume that each laser has a known intrinsic quality-factor, and that the mirror grating is designed for critical output coupling (intrinsic Q = external Q). As the intra-cavity intensity builds up, TPA and FCA processes become more and more dominant, and introduce excess loss. The rate of this non-linear loss would increase with increasing pump current and would yield a non-linear L-I curve, as can be seen in Fig. 8.

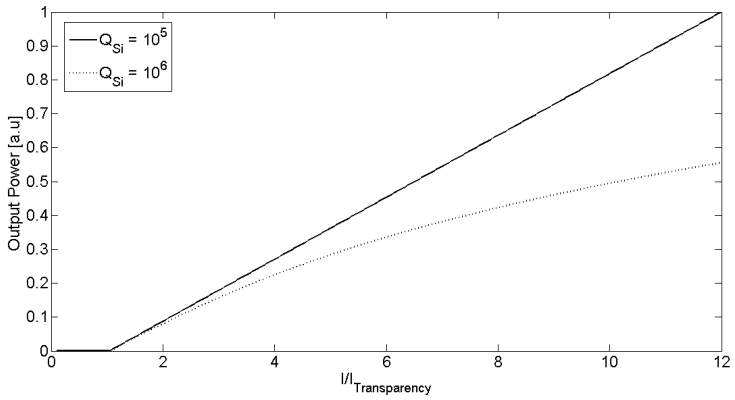

Figure 8: Theoretical L-I curves for different resonator quality factors

The Schawlow–Townes (ST) Linewidth[45] is well understood, and known to be inversely proportional to Q^2 and to the output power. For laser resonator with nominally high quality factor the non-linear loss effectively limits the Q by introducing excess intensity-dependant loss, thus preventing the intra-cavity intensity from rising. As demonstrated in Fig. 9(a), this effect broadens the linewidth compared to the ST linewidth.

The saturation of stored energy due to TPA and FCA also occurs when

[1]Measured experimentally. Measurement technique is beyond the scope of this paper.

the pump current increases, as can be seen in Fig. 8. As a consequence, the linewidth would decrease at a smaller rate than the expected I^{-1}. This can be seen in Fig. 9(b). At high currents TPA causes re-broadening of the linewidth with increased pump current. This is due to the increased total loss by TPA and FCA - the gain has to compensate for the excess non-linear loss by increasing the QW carrier density. This, in turn, increases the spontaneous emission rate into the mode. This effect is accompanied by the saturation of the stored energy in the cavity to broaden the linewidth at higher currents.

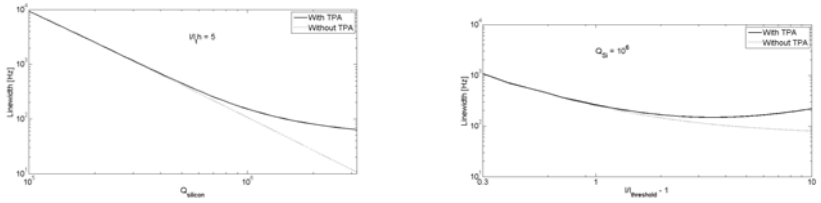

(a) (b)

Figure 9: Effect of TPA on linewidth. (a) ST linewidth vs. Q with and without TPA at 5 times threshold. (b) ST linewidth vs. injection current with and without TPA at Q=10^6

We have fabricated ultra narrow-linewidth lasers on the hybrid Si/III-V platform. The high-Q Si resonator was implemented using a 1-D modulated photonic grating. A distributed defect was used to support a high-Q mode with low radiation losses. This design and fabrication process has yielded[31] resonators of Q as high as 10^6.

Unpatterend III-V epi-structure (InP substrate, InGaAsP QWs) was bonded to the high-Q Si resonator using direct bonding at 285 °C under pressure of 205 PSI. An 8μm current channel was defined using photo-lithography followed by proton implantation. P-contact metal pads were deposited using lift-off lithography and Ti/Pt/Au e-beam evaporation. Wet chemical Mesa etch followed by n-metal Ge/Au/Ni/Au e-beam evaporation was performed to define the n-contact metal pads. The total Q-factor of the hybrid Si/III-V structure was controlled by modal engineering: Due to the high-Q Si resonator, the degree of overlap of the mode with the higher loss III-V was used to control the total Q. A schematic of the device is shown in Fig. 10, however, the exact design and fabrication details are beyond the scope of this paper.

Lasers of two different quality factors were fabricated and measured. The devices were pumped and output light was collected using an integrating

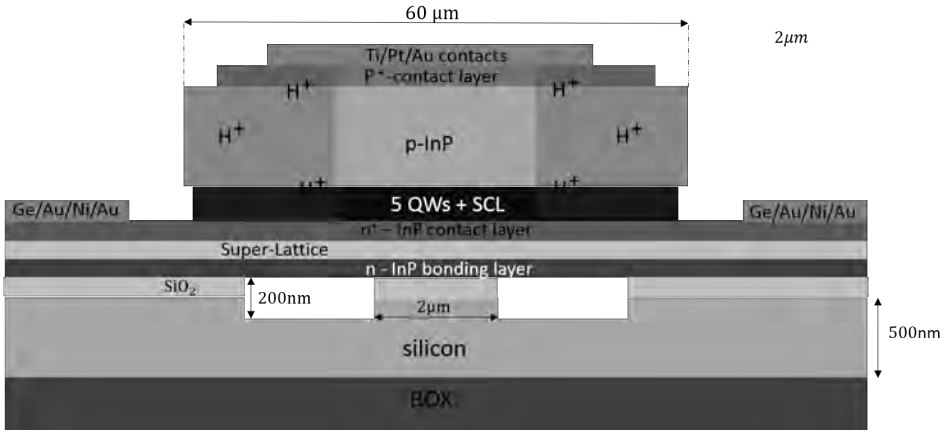

Figure 10: Schematics of the fabricated lasers (not to scale)

sphere. Fig. 11 compares between LI curves of lasers of an estimated Q of 10^5 and $3 \cdot 10^5$. The lower-Q device was measured using a CW current source, while the other device was measured using a pulsed current source. The pulsed current source was used to avoid misinterpretation of thermal roll-off as TPA, since thermal effects might cause the same non-linearity. The short pulse width of $1\mu s$ and duty cycle of 1% ensures that thermal effects are minimal. The L-I curve for the pulsed current source (Fig. 11, solid line) was normalized using the duty cycle, for comparison with the CW measurement (dashed line). The higher-Q device clearly shows a non-linear LI curve, a signature of TPA and subsequent and FCA.

The power spectral density of the frequency noise was measured using an unbalanced Mach-Zehnder interferometer with FSR of 1.56 GHz, and a balanced PD. A feedback loop was used to lock the piezo-driven MZI such that it is in quadrature during the measurement. The Schawlow–Townes linewidth of lasers with the high quality factor was lower than our spectral measurement setup noise floor, and could not be measured. Due to the high-Q operation, the ST white noise floor was masked by $1/f^{\alpha}$ technical noise. Therefore, an experimental equivalent of Fig. 9 could not be produced. However, the high $1/f^{\alpha}$ spectral shape that masked the ST white noise floor can be explained by refractive index fluctuations induced by free-carriers in Si, that are a consequence of TPA. The mathematical justification of this statement is beyond the scope of this paper.

We have studied the effect of two-photon absorption and subsequent

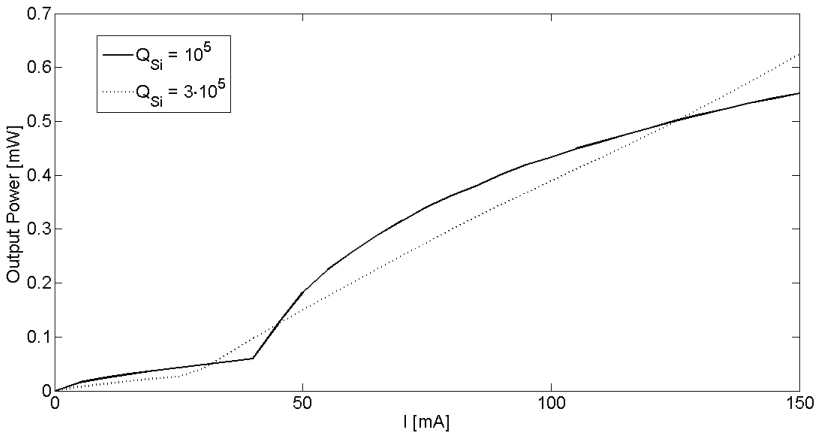

Figure 11: Experimental L-I curve for lasers of different quality factors

free-carrier absorption on the performance of ultra-narrow linewidth hybrid Si/III-V lasers. It was found that these non-linear effects induce a power-dependent reduction of the total cavity quality factor, thus yielding non-linear L-I curves, and reducing the achievable linewidth. The predictions from a non-linear rate equation model were verified experimentally using hybrid Si/III-V lasers of expected quality factor of $3 \cdot 10^5$.

3 Summary

We have proposed a new design paradigm for the semiconductor laser, based on the incorporation of a very high Q resonator as an integral part of the laser cavity, and the removal of light from lossy III-V materials. This is in direct contradiction to a canonical semiconductor laser which has photons both generated and stored in the same, optically lossy, III-V material. We have demonstrated a semiconductor laser with a spectral linewidth of 18 kHz in the telecom band around $1.55\mu m$. Further, we have shown that the large intracavity field intensity resulting from the high-Q operation gives rise to non-linear effects. We have developed a theoretical model based on nonlinear rate equations to study the effect of two-photon absorption and induced free-carrier absorption in silicon on the laser's performance, and compared it to experimental results.

4 Acknowledgments

The authors acknowledge the Army Research Office, the National Science Foundation, and the Defense Advanced Research Projects Agency for financial support, as well as the Kavli Nanoscience Institute at the California Institute of Technology for providing technical and fabrication infrastructure. We are grateful to Prof. John Bowers and his group at the University of California, Santa Barbara for technical assistance.

References

[1] Ogita S, Kotaki Y, Matsuda M, Kuwahara Y, Ishikawa H (1989) Long-cavity, multiple-phase-shift, distributed feedback laser for linewidth narrowing. *Electronics Lett.* 25:629–630.

[2] Soda H, et al. (1987) Stability in single longitudinal mode-operation in GaInAsP-InP phase-adjusted DFB lasers. *IEEE J. Quantum Electronics* 23:804–814.

[3] Ogita S, Kotaki Y, Ishikawa H, Imai H (1988) Optimum design for multiple-phase-shift distributed feedback laser. *Electronics Lett.* 24:731–732.

[4] Okai M, Tsuchiya T, Uomi K, Chinone N, Harada T (1990) Corrugation-pitch-modulated MQW-DFB laser with narrow spectral linewidth (170 kHz). *IEEE Photonics Technology Lett.* 2:529–530.

[5] Liou KY, Dutta NK, Burrus CA (1987) Linewidth-narrowed distributed feedback injection lasers with long cavity length and detuned Bragg wavelength. *Appl. Phys. Lett.* 50:489–491.

[6] Ogita S, Yano M, Ishikawa H, Imai H (1987) Linewidth reduction in DFB laser by detuning effect. *Electronics Lett.* 23:393–394.

[7] Henry CH (1982) Theory of the linewidth of semiconductor lasers. *IEEE J. Quantum Electronics* 18:259–264.

[8] Fang AW, et al. (2006) Electrically pumped hybrid AlGaInAs-Silicon evanescent laser. *Optics Express* 14:9203–9210.

[9] Roelkens G, Thourhout DV, Baets R, Notzel R, Smit M (2006) Laser emission and photodetection in an InP/InGaAsP layer integrated on and coupled to a Silicon-on-Insulator waveguide circuit. *Optics Express* 14:8154–8159.

[10] Fang AW, Lively E, Kuo H, Liang D, Bowers JE (2008) A distributed feedback Silicon evanescent laser. *Optics Express* 16:4413–4419.

[11] Sun XK, et al. (2009) Electrically pumped hybrid evanescent Si/InGaAsP lasers. *Optics Lett.* 34:1345–1347.

[12] Yariv A, Sun X (2007) Supermode Si/III-V hybrid lasers, optical amplifiers and modulators: A proposal and analysis. *Optics express* 15:9147–9151.

[13] Asano T, Song BS, Noda S (2006) Analysis of the experimental Q factors (similar to 1 million) of photonic crystal nanocavities. *Optics Express* 14:1996–2002.

[14] Akahane Y, Asano T, Song BS, Noda S (2003) High-Q photonic nanocavity in a two-dimensional photonic crystal. *Nature* 425:944–947.

[15] Song BS, Noda S, Asano T, Akahane Y (2005) Ultra-high-Q photonic double-heterostructure nanocavity. *Nature Materials* 4:207–210.

[16] Kuramochi E, et al. (2010) Ultrahigh-Q one-dimensional photonic crystal nanocavities with modulated mode-gap barriers on SiO_2 claddings and on air claddings. *Optics Express* 18:15859–15869.

[17] Notomi M (2010) Manipulating light with strongly modulated photonic crystals. *Reports On Progress In Phys.* 73:096501.

[18] Wu MC, Lo YH, Wang S (1988) Linewidth broadening due to longitudinal spatial hole burning in a long distributed feedback laser. *Appl. Phys. Lett.* 52:1119–1121.

[19] Schatz R (1992) Longitudinal spatial instability in symmetrical semiconductor lasers due to spatial hole burning. *IEEE J. Quantum Electronics* 28:1443–1449.

[20] Sorin WV, Chang KW, Conrad GA, Hernday PR (1992) Frequency-domain analysis of an optical FM discriminator. *J. Lightwave Technology* 10:787–793.

[21] Mercer LB (1991) 1/f frequency noise effects on self-heterodyne linewidth measurements. *J. Lightwave Technology* 9:485–493.

[22] Kikuchi K (1987) Impact of 1/f-type FM noise on coherent optical communications. *Electronics Lett.* 23:885–887.

[23] Petermann K (1991) *Laser diode modulation and noise* (Kluwer Academic Publishers, Dordrecht, The Netherlands).

[24] Kikuchi K (1989) Effect of 1/f-type FM noise on semiconductor laser linewidth residual in high-power limit. *IEEE J. Quantum Electronics* 25:684–688.

[25] Hou L, Haji M, Akbar J, Marsh JH (2012) Narrow linewidth laterally coupled 1.55μm AlGaInAs/InP distributed feedback lasers integrated with a curved tapered semiconductor optical amplifier. *Optics Letters* 37:4525–4527.

[26] Kruger U, Petermann K (1988) The semiconductor laser linewidth due to the presence of side modes. *IEEE J. Quantum Electronics* 24:2355–2358.

[27] Satyan N, Vasilyev A, Rakuljic G, Leyva V, Yariv A (2009) Precise control of broadband frequency chirps using optoelectronic feedback. *Optics Express* 17:15991–15999.

[28] H. Park, A. Fang, S. Kodama, and J. Bowers, "Hybrid silicon evanescent laser fabricated with a silicon waveguide and III-V offset quantum wells," *Opt. Express*, vol. 13, pp. 9460–9464, Nov 2005.

[29] S. Stankovic, R. Jones, M. Sysak, J. Heck, G. Roelkens, and D. Van Thourhout, "Hybrid III-V/Si distributed-feedback laser based on adhesive bonding," *Photonics Technology Letters, IEEE*, vol. 24, pp. 2155–2158, Dec 2012.

[30] K. Tanabe, K. Watanabe, and Y. Arakawa, "III-V/Si hybrid photonic devices by direct fusion bonding," *Sci. Rep.*, vol. 2, pp. –, Apr. 2012.

[31] C. T. Santis, S. T. Steger, Y. Vilenchik, A. Vasilyev, and A. Yariv, "High-coherence semiconductor lasers based on integral high-Q resonators in hybrid Si/III-V platforms," *Proceedings of the National Academy of Sciences*, vol. 111, no. 8, pp. 2879–2884, 2014.

[32] A. Griffith, J. Cardenas, C. B. Poitras, and M. Lipson, "High quality factor and high confinement silicon resonators using etchless process," *Opt. Express*, vol. 20, pp. 21341–21345, Sep 2012.

[33] E.-K. Tien, N. S. Yuksek, F. Qian, and O. Boyraz, "Pulse compression and modelocking by using tpa in silicon waveguides," *Opt. Express*, vol. 15, pp. 6500–6506, May 2007.

[34] A. E. Amili, G. Kervella, and M. Alouini, "Experimental evidence and theoretical modeling of two-photon absorption dynamics in the reduction of intensity noise of solid-state Er:Yb lasers," *Opt. Express*, vol. 21, pp. 8773–8780, Apr 2013.

[35] D. Moss, L. Fu, I. Littler, and B. Eggleton, "Ultrafast all-optical modulation via two-photon absorption in silicon-on-insulator waveguides," *Electronics Letters*, vol. 41, pp. 320–321, March 2005.

[36] P. Barclay, K. Srinivasan, and O. Painter, "Nonlinear response of silicon photonic crystal microresonators excited via an integrated waveguide and fiber taper," *Opt. Express*, vol. 13, pp. 801–820, Feb 2005.

[37] T. Visser, H. Blok, B. Demeulenaere, and D. Lenstra, "Confinement factors and gain in optical amplifiers," *Quantum Electronics, IEEE Journal of*, vol. 33, pp. 1763–1766, Oct 1997.

[38] Q. Lin, O. J. Painter, and G. P. Agrawal, "Nonlinear optical phenomena in silicon waveguides: modeling and applications," *Opt. Express*, vol. 15, pp. 16604–16644, Dec 2007.

[39] M. Dinu, F. Quochi, and H. Garcia, "Third-order nonlinearities in silicon at telecom wavelengths," *Applied Physics Letters*, vol. 82, no. 18, pp. 2954–2956, 2003.

[40] H. K. Tsang, C. S. Wong, T. K. Liang, I. E. Day, S. W. Roberts, A. Harpin, J. Drake, and M. Asghari, "Optical dispersion, two-photon absorption and self-phase modulation in silicon waveguides at 1.5um wavelength," *Applied Physics Letters*, vol. 80, no. 3, pp. 416–418, 2002.

[41] J. Zhang, Q. Lin, G. Piredda, R. W. Boyd, G. P. Agrawal, and P. M. Fauchet, "Anisotropic nonlinear response of silicon in the near-infrared region," *Applied Physics Letters*, vol. 91, no. 7, pp. –, 2007.

[42] R. A. Soref and Bria, "Electrooptical effects in silicon," *IEEE Journal of Quantum Electronics*, vol. QE-23, pp. 123–129, January 1987.

[43] D. Dimitropoulos, R. Jhaveri, R. Claps, J. C. S. Woo, and B. Jalali, "Lifetime of photogenerated carriers in silicon-on-insulator rib waveguides," *Applied Physics Letters*, vol. 86, no. 7, pp. –, 2005.

[44] A. Yariv, *Quantum electronics*. Wiley, 3rd ed., 1989.

[45] A. L. Schawlow and C. H. Townes, "Infrared and optical masers," *Phys. Rev.*, vol. 112, pp. 1940–1949, Dec 1958.